

PAPER • OPEN ACCESS

## Excitation of Alfvén eigenmodes by fusion-born alpha-particles in D-<sup>3</sup>He plasmas on JET

To cite this article: V G Kiptily *et al* 2022 *Plasma Phys. Control. Fusion* **64** 064001

View the [article online](#) for updates and enhancements.

### You may also like

- [Simulation of heating and current drive sources for scenarios of the ITER research plan](#)  
Mireille Schneider, Ernesto Lerche, Dirk Van Eester et al.
- [Transport and losses of fusion-born alpha particles in the presence of tearing modes using the new Toroidal Accelerated Particle Simulator \(TAPaS\)](#)  
David Zarzoso, Diego del-Castillo-Negrete, Rémi Lacroix et al.
- [Evidence for Alfvén eigenmodes driven by alpha particles in D-<sup>3</sup>He fusion experiments on JET](#)  
V.G. Kiptily, M. Fitzgerald, Ye.O. Kazakov et al.

# Excitation of Alfvén eigenmodes by fusion-born alpha-particles in D-<sup>3</sup>He plasmas on JET

V G Kiptily<sup>1,\*</sup>, Ye O Kazakov<sup>2</sup>, M Nocente<sup>3,4</sup>, J Ongena<sup>2</sup>, F Belli<sup>5</sup>, M Dreval<sup>6,7</sup>, T Craciunescu<sup>8</sup>, J Eriksson<sup>9</sup>, M Fitzgerald<sup>1</sup>, L Giacomelli<sup>4</sup>, V Goloborodko<sup>10</sup>, M V Iliasova<sup>11</sup>, E M Khilkevitch<sup>11</sup>, D Rigamonti<sup>4</sup>, A Sahlberg<sup>9</sup>, M Salewski<sup>12</sup>, A E Shevelev<sup>11</sup>, J Garcia<sup>13</sup>, H J C Oliver<sup>1</sup>, S E Sharapov<sup>1</sup>, Z Stancar<sup>14</sup>, H Weisen<sup>15</sup> and JET Contributors<sup>16</sup>

<sup>1</sup> United Kingdom Atomic Energy Authority, Culham Centre for Fusion Energy, Culham Science Centre, Abingdon, Oxon OX14 3DB, United Kingdom

<sup>2</sup> Laboratory for Plasma Physics, LPP-ERM/KMS, Partner in the Trilateral Euregio Cluster (TEC), Brussels, Belgium

<sup>3</sup> Dipartimento di Fisica, Università di Milano-Bicocca, Milan, Italy

<sup>4</sup> Institute for Plasma Science and Technology, National Research Council, Milan, Italy

<sup>5</sup> Unità Tecnica Fusione, ENEA C. R. Frascati, via E. Fermi 45, 00044 Frascati (Roma), Italy

<sup>6</sup> Institute of Plasma Physics, National Science Center, Kharkov Institute of Physics and Technology, Kharkov, Ukraine

<sup>7</sup> V.N. Karazin Kharkiv National University, Kharkiv, Ukraine

<sup>8</sup> National Institute for Laser, Plasma and Radiation Physics, Bucharest, Romania

<sup>9</sup> Department of Physics and Astronomy, Uppsala University, SE-75120 Uppsala, Sweden

<sup>10</sup> Kyiv Institute for Nuclear Research, Prospekt Nauky 47, Kyiv 03680, Ukraine

<sup>11</sup> Ioffe Physico-Technical Institute, 26 Politekhnicheskaya, St Petersburg 194021, Russia

<sup>12</sup> Department of Physics, Technical University of Denmark, Kgs. Lyngby, Denmark

<sup>13</sup> CEA—IRFM, 13115 Saint-Paul-lez-Durance, France

<sup>14</sup> Jožef Stefan Institute, Jamova 39, SI-1000 Ljubljana, Slovenia

<sup>15</sup> Ecole Polytechnique Fédérale de Lausanne (EPFL), Swiss Plasma Center (SPC), CH-1015 Lausanne, Switzerland

E-mail: [Vasili.Kiptily@ukaea.uk](mailto:Vasili.Kiptily@ukaea.uk)

Received 4 October 2021, revised 9 March 2022

Accepted for publication 14 March 2022

Published 21 April 2022



CrossMark

## Abstract

Alfvén eigenmode (AE) instabilities driven by alpha-particles have been observed in D-<sup>3</sup>He fusion experiments on the Joint European Torus (JET) with the ITER-like wall. For the efficient generation of fusion alpha-particles from D-<sup>3</sup>He fusion reaction, the three-ion radio frequency scenario was used to accelerate the neutral beam injection 100 keV deuterons to higher energies in the core of mixed D-<sup>3</sup>He plasmas at high concentrations of <sup>3</sup>He. A large variety of fast-ion

<sup>16</sup> See the author list of ‘Overview of JET results for optimising ITER operation’ by J Mailloux *et al* to be published in Nuclear Fusion Special issue: Overview and Summary Papers from the 28th Fusion Energy Conference (Nice, France, 10–15 May 2021).

\* Author to whom any correspondence should be addressed.



Original content from this work may be used under the terms of the [Creative Commons Attribution 4.0 licence](https://creativecommons.org/licenses/by/4.0/). Any further distribution of this work must maintain attribution to the author(s) and the title of the work, journal citation and DOI.

driven magnetohydrodynamic modes were observed, including the elliptical Alfvén eigenmodes (EAEs) with mode numbers  $n = -1$  and axisymmetric modes with  $n = 0$  in the frequency range of EAEs. The simultaneous observation of these modes indicates the presence of rather strong alpha-particle population in the plasma with a ‘bump-on-tail’ shaped velocity distribution. Linear stability analysis and Fokker–Planck calculations support the observations. Experimental evidence of the AEs excitation by fusion-born alpha-particles in the D- $^3\text{He}$  plasma is provided by neutron and gamma-ray diagnostics as well as fast-ion loss measurements. We discuss an experimental proposal for the planned full-scale D-T plasma experiments on JET based on the physics insights gained from these experiments.

Keywords: tokamak, fusion-born alpha-particles, MHD instabilities, fast-ion diagnostics

(Some figures may appear in colour only in the online journal)

## 1. Introduction

In a thermonuclear fusion reactor, the reaction  $\text{D}(\text{T},n)^4\text{He}$  between deuterium (D) and tritium (T) will be the main source of energy.  $^4\text{He}$ -ions (alpha-particles), which are born with an energy of 3.5 MeV, must be well confined to transfer their energy to the plasma particles during their collisional slowing-down and thus to provide the power for a self-sustained D-T burning plasma. It is equally important that additional effects associated with the presence of the alpha-particles should not lead to a detrimental degradation of the plasma confinement. Among these, the possible excitation of magnetohydrodynamic (MHD) modes by fusion-born alpha-particles is of particular importance. Indeed, Alfvén instabilities can significantly influence the fast-ion transport and plasma thermal confinement. This topic is thus of considerable interest for high-Q operation in ITER (e.g. [1] and references therein). Therefore, dedicated alpha-particle studies were undertaken in past D-T experiments on the Tokamak Fusion Test Reactor and the Joint European Torus (JET) [2, 3]. Further alpha-particle physics studies are planned in the forthcoming D-T campaign in JET with the ITER-like wall (JET-ILW) [4]. An important effort of physics understanding is being carried out by performing analyses and modelling of JET experiments with D-plasmas towards an improvement of the understanding of the D-T plasma and fusion-born alpha particle physics [5]. In D-T plasmas, Alfvén eigenmodes (AEs) can be driven by the fusion-born alpha-particles, inducing a significant redistribution and loss of fast-ions. Recent experiments have been conducted in JET D-plasmas in order to prepare scenarios aimed at observing alpha-driven toroidal Alfvén eigenmodes (TAEs) in JET D-T experiments [6].

However, using the newly developed three-ion scenario, we are able to study effects of fusion-born alpha-particles in plasmas without tritium well before the sophisticated full-scale D-T experiments characterised by harsh radiation conditions for diagnostics, using the aneutronic D- $^3\text{He}$  fusion reaction



which generates alpha-particles with an energy very close to those produced in the D-T reaction, albeit with a lower reaction rate. The D- $^3\text{He}$  plasma is still a source of 2.5 MeV

neutrons due to the D-D reaction. For deuteron energies up to  $\sim 4$  MeV, both  $\text{T}(\text{D},n)^4\text{He}$  and  $^3\text{He}(\text{D},p)^4\text{He}$  reactions have non-monotonic cross-sections ( $\sigma$ ) with a maximum for deuteron energies  $E_{\text{D}} \approx 0.11$  MeV and  $\approx 0.44$  MeV, whereas the  $\text{D}(\text{D},n)^3\text{He}$  reaction has a monotonic cross-section [7]. In order to maximise the fusion-born alpha-particle source rate relative to the neutron rate from the D-D fusion, deuteron energies should be in the range  $E_{\text{D}} \approx 0.15\text{--}1$  MeV, where  $\sigma_{\text{D}^3\text{He}} \gtrsim 3\sigma_{\text{D}^2\text{H}}$ .

We carried out fast-ion studies in mixed D- $^3\text{He}$  plasmas using the three-ion D-(D<sub>NBI</sub>)- $^3\text{He}$  radio frequency (RF) scenario [8–10] to accelerate deuterons from the neutral beam injection (NBI) energy ( $\approx 100$  keV) to higher energies resulting in a highly efficient generation of fusion alpha-particles from D- $^3\text{He}$  reactions [11]. The experiments were undertaken at a toroidal magnetic field on axis  $B_0 = 3.7$  T, plasma current  $I_{\text{p}} = 2.5$  MA, central electron densities  $n_{\text{e}0} \approx 5\text{--}7 \times 10^{19} \text{ m}^{-3}$ , at an ICRH frequency  $f = 32.2\text{--}33.0$  MHz using dipole antenna phasing. The cyclotron resonances for thermal D- and  $^3\text{He}$ -ions are located off-axis at the high- and low-magnetic field sides, respectively. Rather large  $^3\text{He}$ -concentrations,  $n_{^3\text{He}}/n_{\text{e}} \approx 20\%\text{--}25\%$ , were purposely chosen to position the ion-ion hybrid (IIH) layer in the plasma core, such that energetic D-ions are generated in the plasma centre. Figure 1(a) shows the RF power deposition computed with the TORIC code [12], which accounts for the poloidal magnetic field and its impact on the propagation and absorption of RF waves in the plasma, illustrating that most of RF power is indeed absorbed in a small region in the plasma core by fast D-NBI ions. Figure 1(b) shows several waveforms of JET pulse #95679 ( $P_{\text{NBI}} \approx 6.9$  MW,  $P_{\text{RF}} \approx 5.8$  MW), in which the central electron temperature increased from 3.6 keV during the NBI-only phase to 7.6 keV in the combined ICRH + NBI phase. The efficient generation of high-energy deuterons with the three-ion scenario resulted in a strongly enhanced neutron rate, increasing from  $\sim 5 \times 10^{14} \text{ s}^{-1}$  to  $\sim 1.0 \times 10^{16} \text{ s}^{-1}$ . The D-D neutron and D- $^3\text{He}$  alpha-particle rates shown in figure 1(b) were simulated by TRANSP [13]. The bottom panel in figure 1(b) shows the time evolution of the  $^3\text{He}$  concentration,  $X[^3\text{He}] = n_{^3\text{He}}/n_{\text{e}} \approx 22\%$ , controlled by the real-time feedback system in JET.

The energy distribution of the RF-accelerated D-NBI ions in these experiments was controlled by varying the

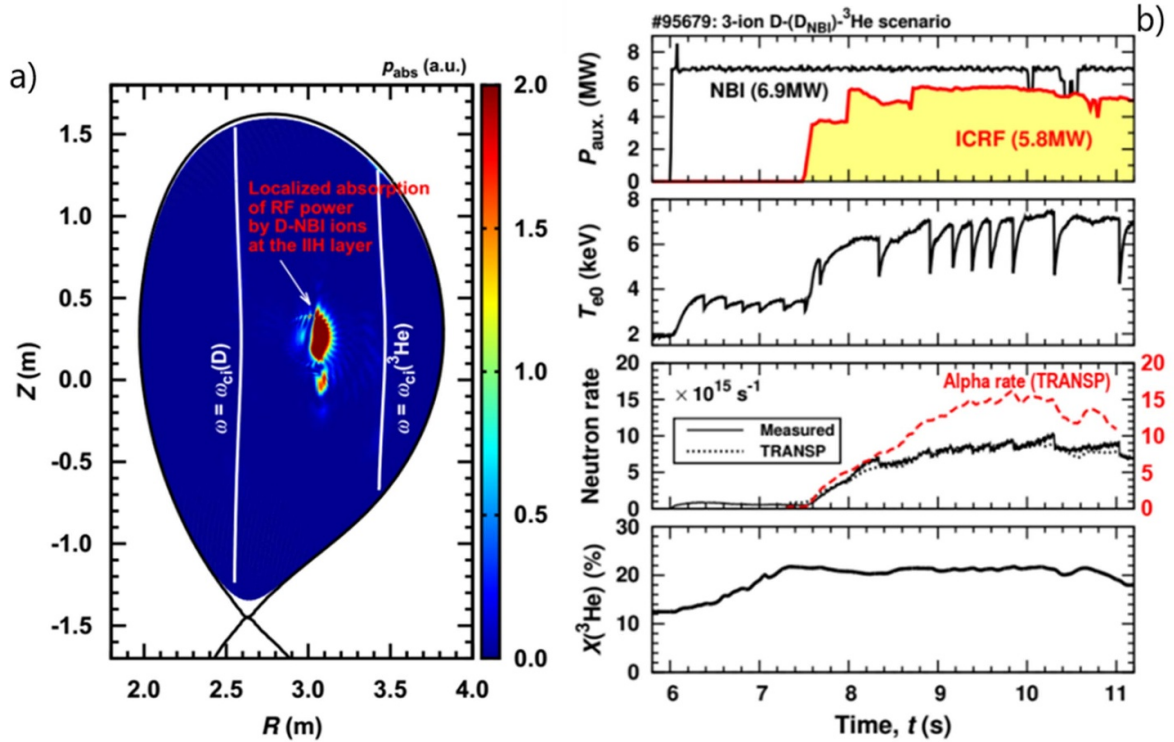


**Figure 1.** (a) The poloidal cross-section of the JET tokamak showing the off-axis location of the cyclotron resonances of <sup>3</sup>He- and D-ions and the core absorption of RF power by fast D-NBI ions in the close vicinity of the I/H layer, as calculated with the TORIC code [12], which accounts for the poloidal magnetic field and the resonance lines are not exactly vertical; (b) an overview of JET pulse #95679. The panels show the auxiliary heating power from NBI and ICRH, the central electron temperature,  $T_{e0}$ , the measured D-D neutron rate (black solid line) vs the TRANSP simulation (black dotted line) and the TRANSP-simulated D-<sup>3</sup>He fusion alpha-particle rate (red dashed line). The bottom panel shows the <sup>3</sup>He concentration controlled by the real-time feedback system.

ratio  $P_{\text{RF}}/P_{\text{NBI}}$ . One can see that with  $P_{\text{RF}} \approx 6$  MW and  $P_{\text{NBI}} \approx 7\text{--}11$  MW, the TRANSP-simulated D-<sup>3</sup>He alpha-particle rate  $R_{\alpha} \sim 1.7 \times 10^{16} \text{ s}^{-1}$  was achieved, corresponding to a fusion power  $P_{\text{D}^3\text{He}} \approx 50$  kW.

The central electron temperature  $T_{e0}$  shows recurrent changes known as sawtooth oscillations. It is well-known that the presence of fast-ions in the plasma has a stabilising effect on sawtooth oscillations [14]. However, after long sawteeth a steep and fast drop in  $T_{e0}$  occurs—a so-called sawtooth crash—when a certain stability threshold is crossed [15]. This then leads to a redistribution of the fast-ions in the plasma. Depending on  $P_{\text{ICRF}}$  and  $P_{\text{NBI}}$  and other operational parameters, the sawtooth period  $\Delta t_{\text{ST}}$  in our experiments varied from  $\sim 150\text{--}300$  ms to  $\sim 3.9$  s, the so-called ‘monster’ sawtooth.

A large variety of fast-ion driven MHD modes such as TAEs, elliptical Alfvén eigenmodes (EAEs) and reversed shear Alfvén eigenmodes [16] with different toroidal mode numbers  $n$ , including axisymmetric  $n = 0$  AEs, were observed in these JET-ILW experiments. The excitation of most of these AEs can be explained by resonant wave–particle interactions with a population of ICRF-generated fast D-ions. However, the simultaneous observation of  $n = -1$  and  $n = 0$  modes in the EAE frequency range implies the presence of a fast-ion population in the plasma with a large fraction of highly energetic counter-passing ions (parallel velocity  $v_{\parallel} < 0$ ), together with a positive gradient in the fast-particle energy distribution

function  $\partial f/\partial E > 0$ . A combined fast-ion and MHD analysis shows that the ICRF-generated fast D-ions are not capable to excite  $n = -1$  EAEs. Instead, we show that these AEs with toroidal numbers  $n = 0$  and  $n = -1$  are driven by fusion-born alpha-particles in the JET plasma [17].

The paper is organised as follows. Diagnostics used for fast-ion measurements are described in the next section. The experimental evidence for the observed AEs instabilities driven by fusion-born alpha-particles are presented in section 3. Results of the linear stability analysis and Fokker-Planck calculations are summarised in sections 4 and 5. In the summary and conclusions section, we discuss an extension of our results to D-T plasmas.

## 2. Fast-ion diagnostics

The fast-ion diagnostics set on JET allows us to study confined and escaping fast-ions, including fusion-born alpha-particles. Confined fast-ions are diagnosed with gamma-ray spectrometry [18, 19]. This diagnostic detects gamma-rays that are born in nuclear reactions between confined fast-ions and fuel ions or beryllium, which is the main intrinsic low-Z impurity in JET-ILW plasmas. The gamma-ray diagnostic provides information on the spatial distribution of fast-ions and the MeV range fast-ion energy tail. The gamma-ray energy spectra

were recorded by a collimated LaBr<sub>3</sub> scintillation detector with a tangential LoS in the midplane of the torus [20].

For the fast D-ion energy assessments we used a high-resolution gamma-ray spectrometer based on the high-purity germanium detector (HpGe). This spectrometer views the plasma along a vertical LoS, through the plasma centre ( $R = 2.96$  m) perpendicular to the toroidal field. It has a relative efficiency of  $\approx 95\%$  and an energy resolution of  $\approx 0.2\%$ , ( $\Delta E_{\text{FWHM}} \approx 2.6$  keV at  $E_\gamma = 1332.5$  keV). This high resolution allows measurements of the Doppler gamma-ray line broadening due to kinematics of nuclear reactions between fast-ions and low-Z impurities and thus to infer an effective fast-ion energy [21, 22] and even a measurement of the two-dimensional (2D) fast-ion velocity distribution function by integrated data analysis [23].

Losses were observed with the fast-ion loss detector (FILD) located below the mid-plane ( $Z \approx -0.28$  m) [24]. The light from the FILD scintillator plate (the characteristic scintillator decay-time of  $\approx 0.5$   $\mu\text{s}$ ), transmitted with a coherent optical fibre-bundle is equally split between a charge-coupled device (CCD camera) and a  $4 \times 4$  array of photo-multiplier tubes (PMTs). The PMT array delivers fast signals digitized with 2 MHz rate. The CCD camera provides time-resolved information ( $\Delta t \approx 20$  ms) on the lost-ion pitch-angle,  $\theta = \cos^{-1}(v_{\parallel}/v)$ , between  $35^\circ$  and  $85^\circ$  with a resolution  $\sim 5\%$  and gyro-radius,  $\rho_{\text{gyr}}$ , in the range 3–14 cm with a resolution  $\sim 15\%$ . The major radius at the ion bounce reflection and the pitch-angle  $\theta$  of the grid are related by  $R(\theta) = R_{\text{FILD}} \sin^2 \theta$ , where  $R_{\text{FILD}} = 3.825$  m is the radial position of the FILD scintillator in the vessel. The energy of ions ( $Z_i, A_i$ ) is related to the gyro-radius as  $E_i = [\rho_{\text{gyr}}(\text{cm}) B_{\text{FILD}}(\text{T}) / 14.45]^2 (Z_i^2 / A_i)$ , where  $B_{\text{FILD}}$  is magnetic field at the location of the FILD scintillator plate, which in the presented case, 2.874 T. The grid, ( $\rho_{\text{gyr}}, \theta$ ), used to interpret measurements from the scintillator plate is calculated from the EFIT equilibrium.

The D-D fusion neutrons are measured with the TOFOR spectrometer [25] and the 2D neutron camera (a neutron profile monitor) [26]. TOFOR is a time-of-flight spectrometer for measurements of the neutron emission of the deuterium plasma with different auxiliary heating scenarios, which views the plasma centre ( $\approx 2.74$ – $3.02$  m) vertically. The 2D neutron camera consists of two collimated fan-shaped arrays of NE213 detectors with ten horizontal and nine vertical lines of sight.

### 3. Experimental observations

Gamma-ray measurements provide strong evidence for fusion alpha-particle production in these experiments. Figure 2(a) depicts the gamma-ray spectrum recorded by the tangential spectrometer in discharge #95679. It was identified that events recorded in the energy range 12–17 MeV originate from the  ${}^3\text{He}(\text{D}, \gamma){}^5\text{Li}$  reaction, which is a weak proportional branch ( $\sim 10^{-5}$ ) of the  ${}^3\text{He}(\text{D}, p){}^4\text{He}$  fusion reaction. Also, the  ${}^9\text{Be}(\text{D}, n\gamma){}^{10}\text{B}$  and  ${}^9\text{Be}(\text{D}, p\gamma){}^{10}\text{Be}$  reactions give rise to gammas, which are clearly seen in the rescaled spectrum of figure 2(b). Hence, we can conclude that there is a D-ion

population with energies in the range  $E_D \gtrsim 0.5$  MeV, where the reaction cross-sections are soaring up [7].

The high-resolution gamma-ray HpGe-spectrometer provides further information on the effective energy of the accelerated D-ions in the plasma centre, which is in the field of view of this collimated detector. The HpGe gamma-ray spectrum recorded for  $t = 8.5$ – $11.5$  s in this discharge is presented in figure 3(a). The gamma-ray peaks related to the  ${}^9\text{Be}(\text{D}, n\gamma){}^{10}\text{B}$  and  ${}^9\text{Be}(\text{D}, p\gamma){}^{10}\text{Be}$  reactions are broadened due to the Doppler effect. In addition, a broadened gamma-ray peak at  $E_\gamma = 4439$  keV, which is related to the  ${}^9\text{Be}(\alpha, n\gamma){}^{12}\text{C}$  reaction, indicates the presence of confined fusion-born alpha-particles [18] in the plasma centre. Note that the line at  $E_\gamma = 2223$  keV is rather narrow; this gamma-ray line does not originate from nuclear reactions in the plasma but is related to background gamma-rays from the polyethylene neutron-attenuator bricks placed in front of the detector.

The energy of gamma-rays emitted by the recoil compound nucleus in a nuclear reaction can be expressed as  $E_\gamma \approx E_\gamma^0 [1 + (V_R/c) \cos \theta_\gamma]$ , where  $E_\gamma^0$  is energy of the gamma-ray transition in the recoil nucleus,  $V_R/c \approx 0.046 \sqrt{m_f E_f (\text{MeV}) / M_R}$  is the ratio of the recoil velocity of the excited compound recoil nucleus with mass number  $M_R$  to the speed of light  $c$ ,  $\theta_\gamma$  is the angle between the velocity of fast-ion with mass number  $m_f$  and the axis of the collimated detector. Figure 3(b) shows a fragment of the experimental spectrum with the 2872 keV line and the best Gaussian fit to the data. Note that this line appears in the spectrum due to deexcitation of the  ${}^{10}\text{B}^*$  nucleus excited in the  ${}^9\text{Be}(\text{D}, n\gamma){}^{10}\text{B}^*$  reaction. Taking into account the energy resolution of the spectrometer of  $\approx 5$  keV, the obtained Gaussian broadening width ( $2\sigma$ ) of  $\approx 29 \pm 3$  keV, results in  $\langle E_D \rangle \gtrsim 0.7$  MeV for the energy of the fast D-ions averaged over the sawtooth period. This represents a lower limit for  $\langle E_D \rangle$  considering that the fast D-ions are trapped, i.e. their pitch  $v_{\parallel}/v = 0$ . Note that this is a first order assessment of the average fast D-ion energies and a much more detailed Doppler shape analysis will be published in the future.

Discharge #95679 was simulated by TRANSP [27] coupled with the external heating modules NUBEAM [28] and TORIC and prepared with the OMFIT integrated modelling platform [29]. As input to TRANSP we used electron density and temperature profiles obtained from high resolution Thomson scattering and electron cyclotron emission data. Supported by charge exchange measurements we set the ion temperature profile equal to the electron temperature profile. The plasma equilibrium and safety factor used in the simulations was provided by an EFIT++ equilibrium reconstruction, constrained by magnetics and realistic pressure profiles, i.e. including kinetic profiles as well as the contribution from the RF accelerated fast-ion population. The same equilibrium was used for mapping of the profile data. The concentration of  ${}^3\text{He}$  in the plasma, prescribed as a fraction of the electron density, was based on real-time measurements of the JET tokamak control system. The impurity content was assumed to be 0.9% Be with the remainder ascribed to Ni based on a quasi-neutrality calculation constrained by the measured effective-charge,  $Z_{\text{eff}}$ , from visible spectroscopy.



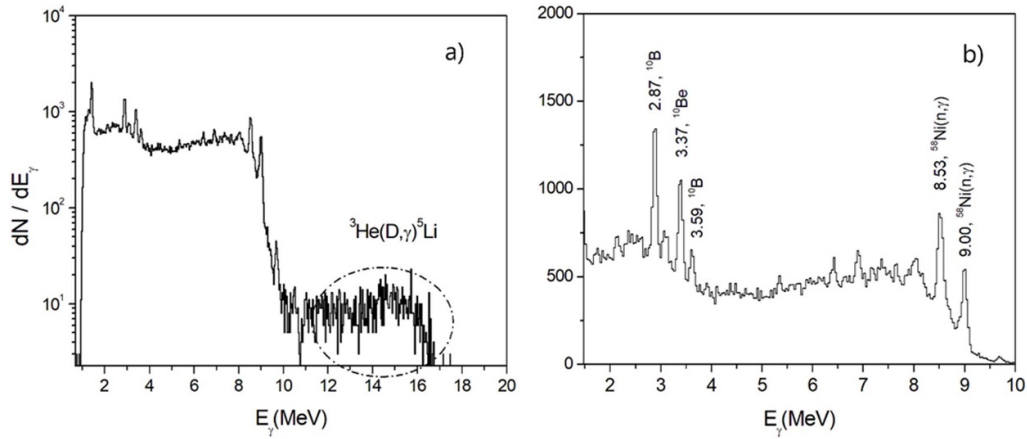


**Figure 2.** Gamma-ray spectrum recorded by the LaBr<sub>3</sub> detector in discharge #95679: (a) a log-scale spectrum displays the detected 17 MeV gammas and (b) a linear-scale zoomed spectrum clearly showing the gammas from the  ${}^9\text{Be}(\text{D},\gamma){}^{10}\text{B}$  and  ${}^9\text{Be}(\text{D},p\gamma){}^{10}\text{Be}$  nuclear reactions.

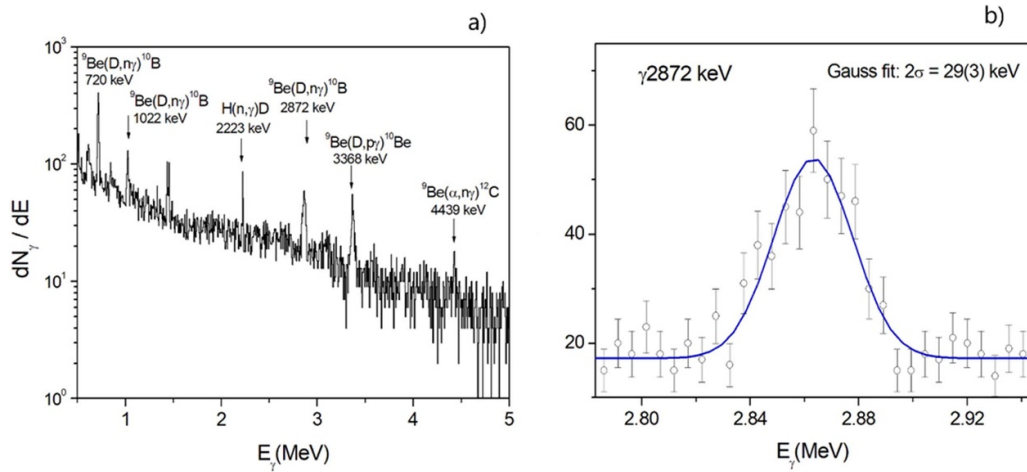


**Figure 3.** (a) Gamma-ray spectrum recorded by HpGe-detector for  $t = 8.5\text{--}11.5$  s of JET discharge #95679; (b) experimental data together with the best Gaussian fit for the Doppler broadened gamma-ray line 2872 keV from the  ${}^9\text{Be}(\text{D},\gamma){}^{10}\text{B}$  reaction.

The TRANSP simulations show that most of the fast deuterons in our experiments have a pitch-angle  $\theta \approx 50^\circ\text{--}60^\circ$ , or pitch parameter  $\lambda = v_{\parallel}/v \approx 0.5\text{--}0.65$ , in the energy range  $E_D \approx 0.5\text{--}1.25$  MeV. These results are consistent with the Doppler broadening measurements, i.e. for the fast D-ion pitch angles predicted by TRANSP the energy  $\langle E_D \rangle \approx 0.9\text{--}1.1$  MeV. The radial profile of the alpha-particle density after slowing-down computed with TRANSP confirms the strong core localisation of the fusion-born alpha-particles. This simulation and the Doppler broadening measurements agree rather well with neutron spectrometry results, i.e. the TOFOR spectra analysis (figure 4(c)) indicates that the energy of the fast D-ions in the plasma centre below 2.7 MeV in this discharge.

The velocity-space sensitivity of fusion product measurements can be assessed with weight functions [30, 31]. For TOFOR the observed velocity space for the time-of-flight  $t_{\text{ToF}} = 46$  ns is shown in figure 4(b), where all detected neutrons for the given time-of-flight originate from the

coloured region. We did not consider neutron detections with times-of-flight less of 42 ns, the range where a random coincidence background is dominant. For the TOFOR setup energy of detected neutrons related to  $t_{\text{ToF}}$  as  $E_n$  (MeV)  $\approx [100/t_{\text{ToF}}(\text{ns})]^2$ . Energetic deuterons resulting in a detection of a neutron with a time-of-flight of 46 ns have energies of at least 1.5 MeV. The energy sensitivity of the different times-of-flight can be estimated by integration of the weight functions over pitch. Here, we integrated over pitches parameter  $\lambda = v_{\parallel}/v$  from  $-0.55$  to  $+0.55$ , where sensitivity of the TOFOR weight functions is rather high. Figure 4(c) shows a comparison of the energy sensitivity of the different times-of-flight. One can see that the maximum deuteron energies is situated in the range 1.5–2.7 MeV.

Gamma-ray emission from the  ${}^9\text{Be}(\text{D},n\gamma){}^{10}\text{B}$  and  ${}^9\text{Be}(\text{D},p\gamma){}^{10}\text{Be}$  reactions recorded with tangential spectrometer indicates significant changes in the energy distribution of the fast D-ions that could be attributed to sawtooth crashes in the reported discharges. A solid variation of the gamma-ray

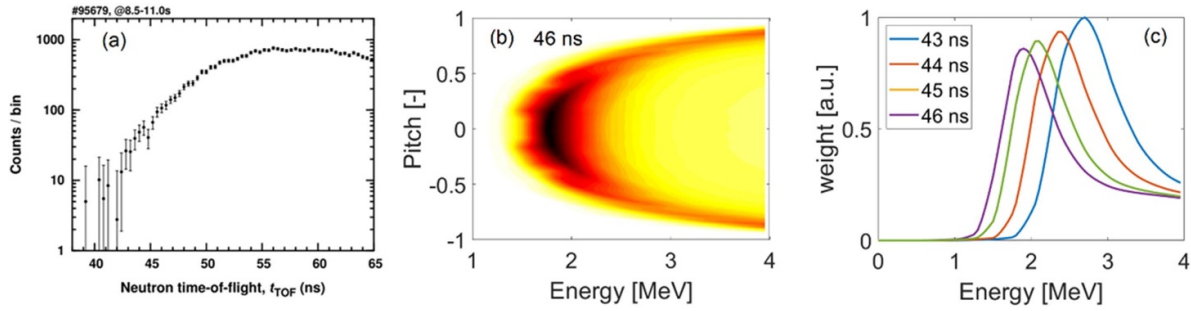


**Figure 4.** (a) Neutron time-of-flight spectrum recorded in discharge #95679 by TOFOR; (b) TOFOR weight function calculated in  $(E_D, \lambda)$ -space for the time-of-flight 46 ns; (c) TOFOR weight functions integrated over pitch for several time-of-flights.

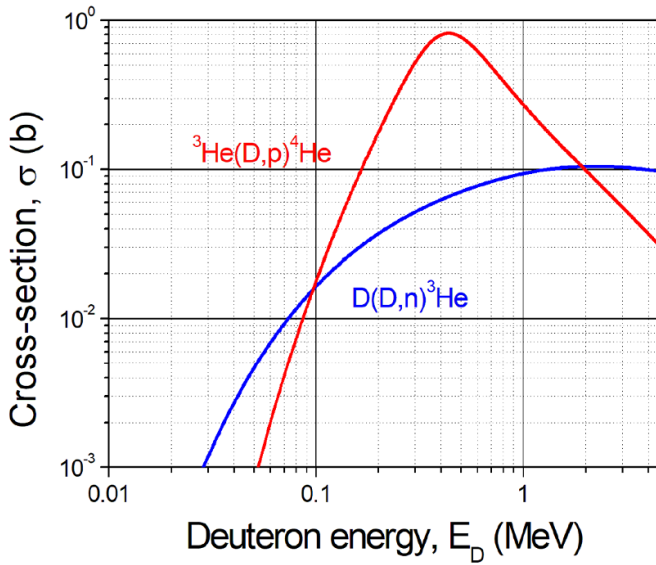


**Figure 5.** Cross-sections of the  ${}^3\text{He}(\text{D},\text{p}){}^4\text{He}$  and  $\text{D}(\text{D},\text{n}){}^3\text{He}$  reactions [7].

line intensities in discharge #95679 can be explained by the fast-growing cross-section of the  ${}^9\text{Be}(\text{D},\text{n}\gamma){}^{10}\text{B}$  reaction in the energy range  $E_D \sim 0.2\text{--}2$  MeV.

This considerable energy redistribution of the fast D-ion population due to sawtooth crashes lead to changes of the alpha-particle source because the  ${}^3\text{He}(\text{D},\text{p}){}^4\text{He}$  reaction cross-section (see figure 5) is highly non-monotonic around  $E_D \approx 0.4$  MeV. Indeed, the intensity of the 17 MeV gamma-rays from the  ${}^3\text{He}(\text{D},\gamma){}^5\text{Li}$  reaction shows clear variations that are correlated with the sawtooth crashes, from which we infer a modulation in the production rate of the alpha-particles. Figure 6 demonstrates relative changes of intensity of the 17 MeV gammas as function of time in discharge #95679. These variations are correlated with changes in the integral neutron emissivities recorded by both the central and outer channels of the neutron camera. Indeed, for the first four sawtooth crashes in the figure, the  $\text{D}-{}^3\text{He}$  fusion rate increases quite strongly (indicated by the black full lines), while at the same time the relative D-D fusion rate slightly drops. For the following three sawteeth, the D-D reaction rate is growing with increase of the sawtooth period,  $\Delta t_{\text{ST}}$ , but the

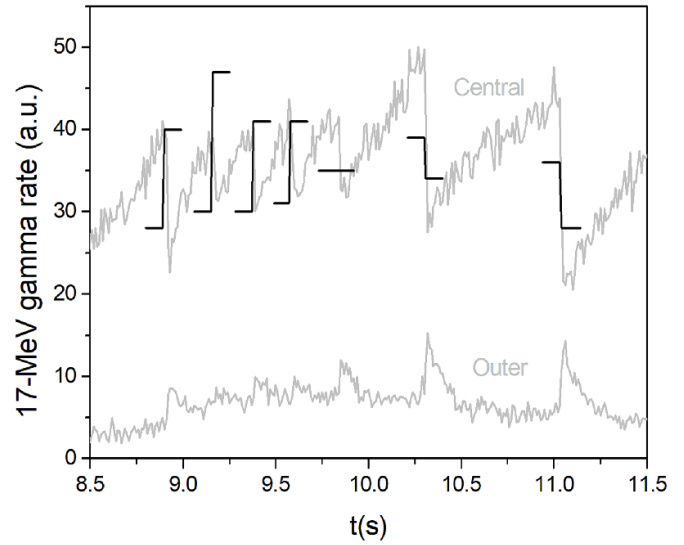


**Figure 6.** Line-integrated emissivity of the neutron camera central and outer channels (grey lines) and changes in the 17 MeV gamma-ray intensity (black lines) 100 ms before and after the sawtooth crashes.

${}^3\text{He}(\text{D},\gamma){}^5\text{Li}$  reaction rate, i.e. the  $\text{D}-{}^3\text{He}$  fusion rate, drops after crashes. This effect could be explained by both changes in the energy distribution of the fast D-ions and the specific energy dependence of the reaction cross-sections shown in figure 5. During the long sawteeth with  $\Delta t_{\text{ST}} \approx 0.46$  and  $\approx 0.73$  s, D-ions are accelerated by RF to higher energies than during sawteeth with shorter periods  $\Delta t_{\text{ST}} \approx 0.20\text{--}0.25$  s. For energies  $E_D \gtrsim 0.5$  MeV the  $\text{D}(\text{D},\text{n}){}^3\text{He}$  cross-section is monotonically increasing with energy, while the cross-section for the  ${}^3\text{He}(\text{D},\text{p}){}^4\text{He}$  reaction (and similar for  ${}^3\text{He}(\text{D},\gamma){}^5\text{Li}$  reaction) is decreasing. The  ${}^3\text{He}(\text{D},\text{p}){}^4\text{He}$  cross-section significantly exceeds that of the  $\text{D}(\text{D},\text{n}){}^3\text{He}$  reaction in the energy range  $0.2 \lesssim E_D \lesssim 1$  MeV. The ratio of the cross-sections of the  ${}^3\text{He}(\text{D},\text{p}){}^4\text{He}$  and  $\text{D}(\text{D},\text{n}){}^3\text{He}$  reactions changes dramatically with  $\langle E_D \rangle$ , as clearly shown by the ratios  $(0.5 \text{ MeV}):(1 \text{ MeV}):(1.9 \text{ MeV}):(2.5 \text{ MeV}) \approx 11:3:1:0.7$ . Hence, the 17 MeV gamma-ray modulation (and the alpha-particle source rate) depends on the variations in the energies of the fast D-ions modulated by the sawteeth. Depending on  $\Delta t_{\text{ST}}$  and the slowing down time,  $\tau_D$  of the fast D-ions, the

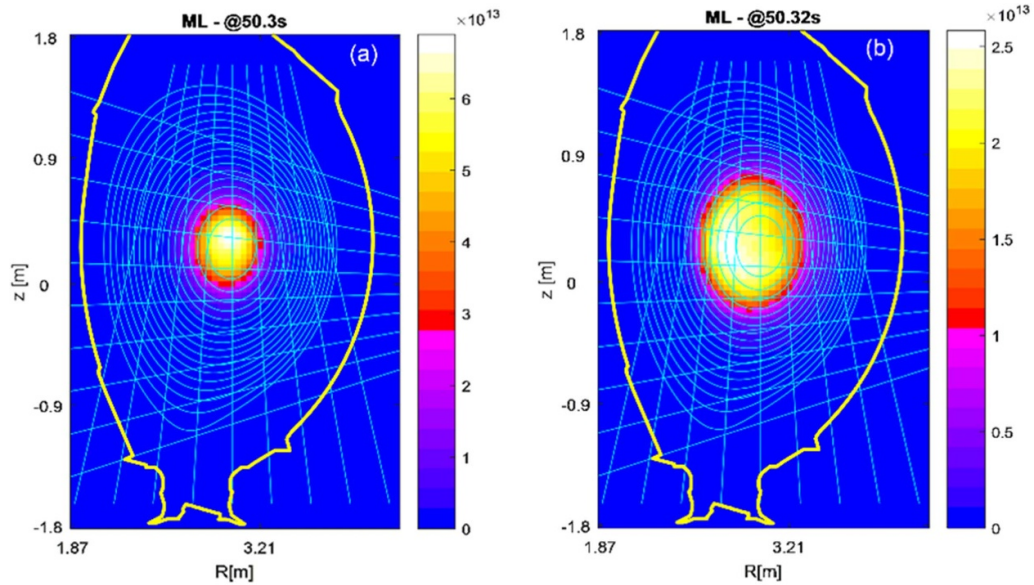


**Figure 7.** 2D tomographic reconstruction of the neutron emissivity of the D-D fusion reaction obtained with 2D neutron camera for discharge #95679: (a)—tomographic reconstruction of line-integrated emissivities recorded 10 ms before the sawtooth crash at 10.31 s and (b)—10 ms afterwards. The colour scale is normalised.

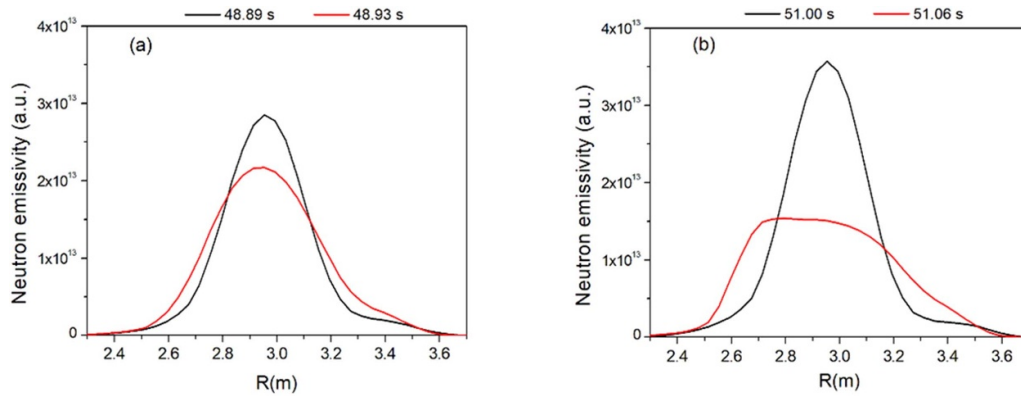


**Figure 8.** Neutron emission profiles for discharge #95679 in the equatorial plane in JET ( $Z = 0$ , i.e. LoS of tangential gamma-ray spectrometer) obtained from the tomographic reconstruction for short (a) and long (b) sawteeth; black lines—10 ms before crash, red lines—10 ms after crash.

sawtooth crashes lead to different modulation amplitudes of the  ${}^3\text{He}(\text{D},\gamma){}^5\text{Li}$  (and  ${}^3\text{He}(\text{D},p){}^4\text{He}$ ) reaction rate.

Together with variations in the energy of the fast D-ions, the sawtooth crashes also lead to a significant spatial redistribution of fast-ions, resulting in an expulsion of the fast D-ions from the plasma centre to the outer region. This explains the drops in the neutron rate in the central channels of the 2D camera and the increase in the outer channels in figure 6.

The tomographic reconstruction of the line-integrated emissivity signals from the 2D neutron camera clearly demonstrates that the strongly localized D-D fusion source before the sawtooth crash (figure 7(a)) is broadened after the crash (figure 7(b)). Thus, the post-crash central neutron emission is significantly reduced in the plasma centre.

Analysis of the neutron camera profiles indicates the differences in the spatial redistribution of the fast D-ions caused by the crashes after short and long sawteeth. Indeed, the

broadening of the neutron emissivity profiles is much less for crashes after short sawteeth (figure 8(a)) than after long sawteeth (figure 8(b)). We conclude that the impact of the spatial redistribution of the fast D-ions on the measured  ${}^3\text{He}(\text{D},\gamma){}^5\text{Li}$  reaction rate, proportional to the alpha-particle generation rate, is quite significant. Also, fast D-ions can appear in the loss cone region due the spatial redistribution caused by sawtooth crashes.

Massive sawtooth induced losses of the RF-accelerated D-ions and D- ${}^3\text{He}$  alpha-particles have been observed in these experiments. Figure 9(a) represents a typical FILD footprint of the first-orbit losses of fusion-born alpha-particles in discharge #94698 just before the monster sawtooth crash at 10.53 s. The gyro-radius of the lost ions exceeds  $\approx 8$  cm, corresponding to energies for the lost alpha-particles  $E_\alpha \gtrsim 2.5$  MeV. This agrees with the alpha-particle birth energy spectra shown in figure 10(b) calculated with the Monte-Carlo code GENESIS



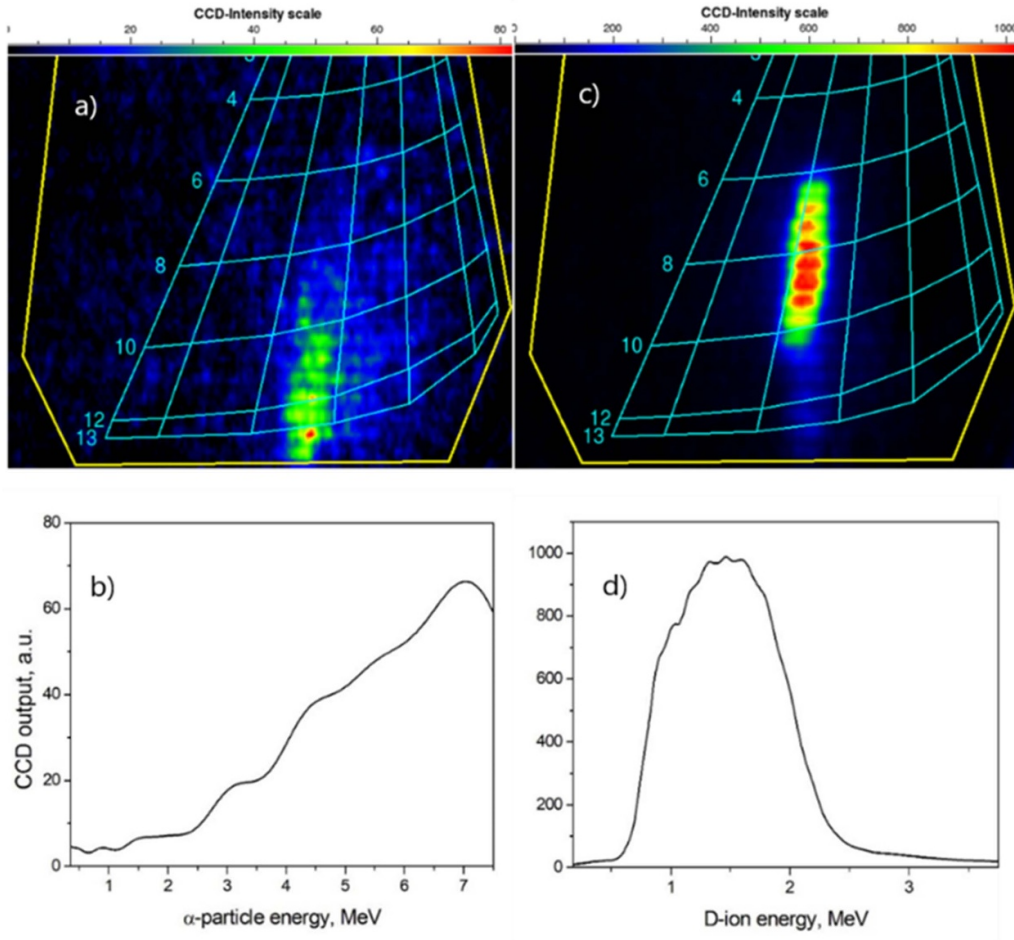


**Figure 9.** FILD data obtained in discharge #94698 at the monster sawtooth at 10.53 s: (a) footprint of losses recorded before the sawtooth crash; (b) losses at pitch-angle  $\theta = 57.5^\circ$  versus alpha-particle energy recorded before the sawtooth crash; (c) footprint of losses recorded during the sawtooth crash; (d) losses at pitch-angle  $\theta = 52.75^\circ$  versus D-ion energy recorded during the sawtooth crash.

[32], which used as input the distribution function for the fast D-ions calculated by TRANSP (see figure 10(a)) and extended D-<sup>3</sup>He fusion cross-sections [33, 34]. These calculations reveal that the RF-accelerated D-beam ion distribution function responsible for the broad alpha-particle birth spectrum, with energies in between 2 and 6 MeV, depending on the value for the pitch parameter  $\lambda$ . This justifies attributing the measured fast ion losses with large gyro-radii to fusion-born alpha-particles. So, the energy distribution of alpha-particle losses with pitch-angle  $\theta \approx 57.5^\circ$  presented in figure 9(b) corresponds closely to the calculated alpha-particle energy spectra at  $\lambda = +0.5$  (see figure 10(b)).

Figure 9(c) depicts the loss footprint during the monster sawtooth crash. The FILD loss signal is very strong and distributed along the pitch-angle  $\theta \approx 52.5^\circ$  that is related to the trapped-passing boundary in the orbit phase-space. This suggests indeed that the substantial spatial redistribution of the fast D-ions can explain the losses observed. Using the FILD data we obtained the energy distribution of the lost D-ions shown in figure 9(d). The energy range, 0.7–2.4 MeV, of the lost D-ions is consistent with the gamma-ray and neutron measurements as well as the TRANSP simulations (see figure 10(a)). Orbits of lost fast D-ions and alpha-particles,

calculated backward-in-time from hot-spots on the FILD scintillation plate, are represented in figure 11. The figure shows that lost alpha-particles originate from the plasma centre, whereas the lost D-ion orbits intersect the sawtooth inversion radius  $q = 1$  at the radius  $R \approx 3.25 \pm 0.05$  m (obtained with ECE diagnostics).

We observed a rich variety of fast-ion driven AEs, including TAEs, EAEs as well as Alfvén cascades. Like past fast-ion experiments with ICRF on JT-60U [35], the behaviour of TAEs and EAEs was correlated with sawtooth dynamics. In our experiments EAEs were mostly observed during phases with short sawteeth. In each of these discharges (see main plasma parameters in the table 1), a monster sawtooth crash facilitated the excitation of EAEs; under these conditions, the delay between the start of EAE activities after the monster sawtooth crash was typically  $\sim 80$ – $100$  ms (see figure 12).

The observed EAEs are located at the  $q = 1$  surface, as is inferred from correlation reflectometer measurements. They consist of two counter-propagating poloidal modes with mode numbers  $m_1 = n - 1$  and  $m_2 = n + 1$ .

The destabilization of AEs is only possible when the mode drive by fast ions is sufficiently large and overcomes mode damping. Alfvénic instabilities are usually driven unstable by

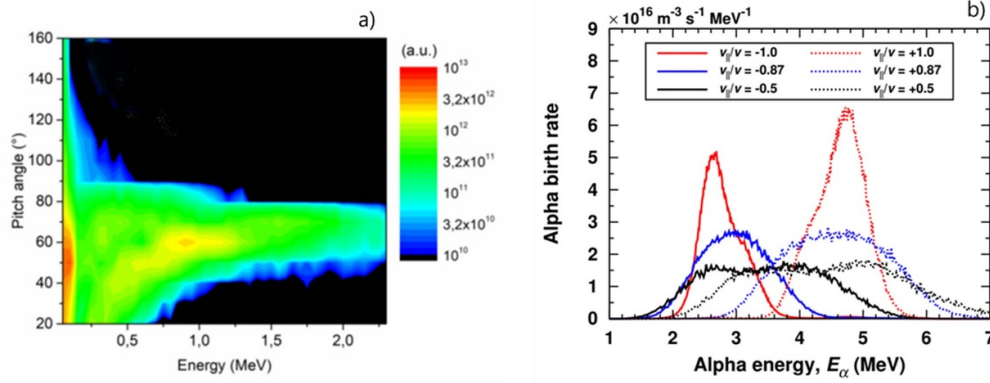


**Figure 10.** (a) Pitch-angle versus energy distribution of the D-ions from TRANSP in JET discharge #95679; (b) the birth energy spectra of the D-<sup>3</sup>He fusion-born alpha-particles obtained with the code GENESIS using as input the distribution function of ICRF-accelerated D-ions (a) calculated with TRANSP.

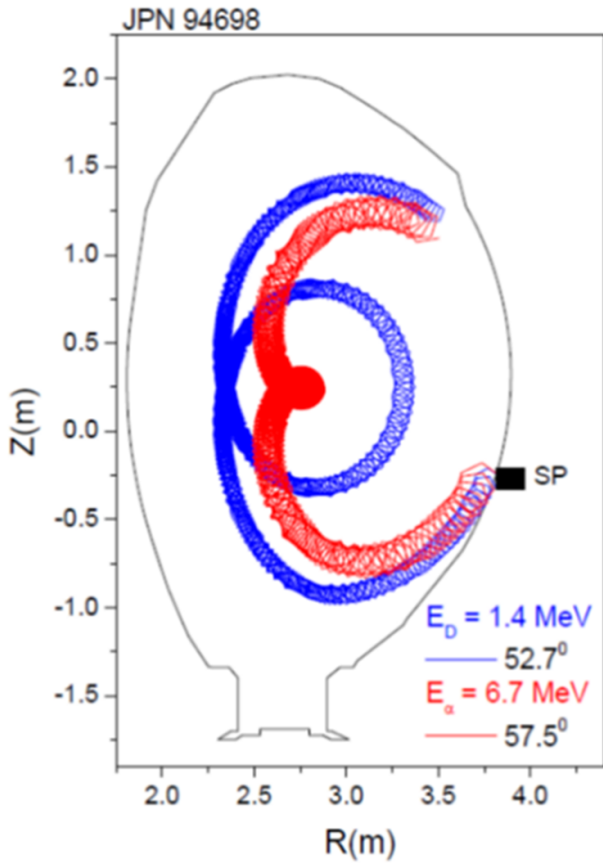


**Figure 11.** Orbits of lost fast ions calculated backward-in-time from the FILD scintillator plate: red line—alpha-particle orbit with  $E_\alpha = 6.7$  MeV and  $\theta = 57.5^\circ$ ; blue line—D-ion orbit with  $E_D = 1.4$  MeV and  $\theta = 52.7^\circ$ ; these parameters are related to the footprints presented in figure 9.

the free energy in the spatial gradient of the distribution function of energetic ions. The peaked pressure profile of fast D ions provides a positive term for the destabilization of modes with  $n > 0$ . Yet, the same mechanism provides damping, rather

than a drive, for modes with  $n < 0$ . Thus, other drive mechanisms are required for the destabilization of the observed  $n = -1$  mode. Possible mechanisms include the anisotropy of the distribution function with respect to the pitch angle and the bump-on-tail mechanism, as discussed further.

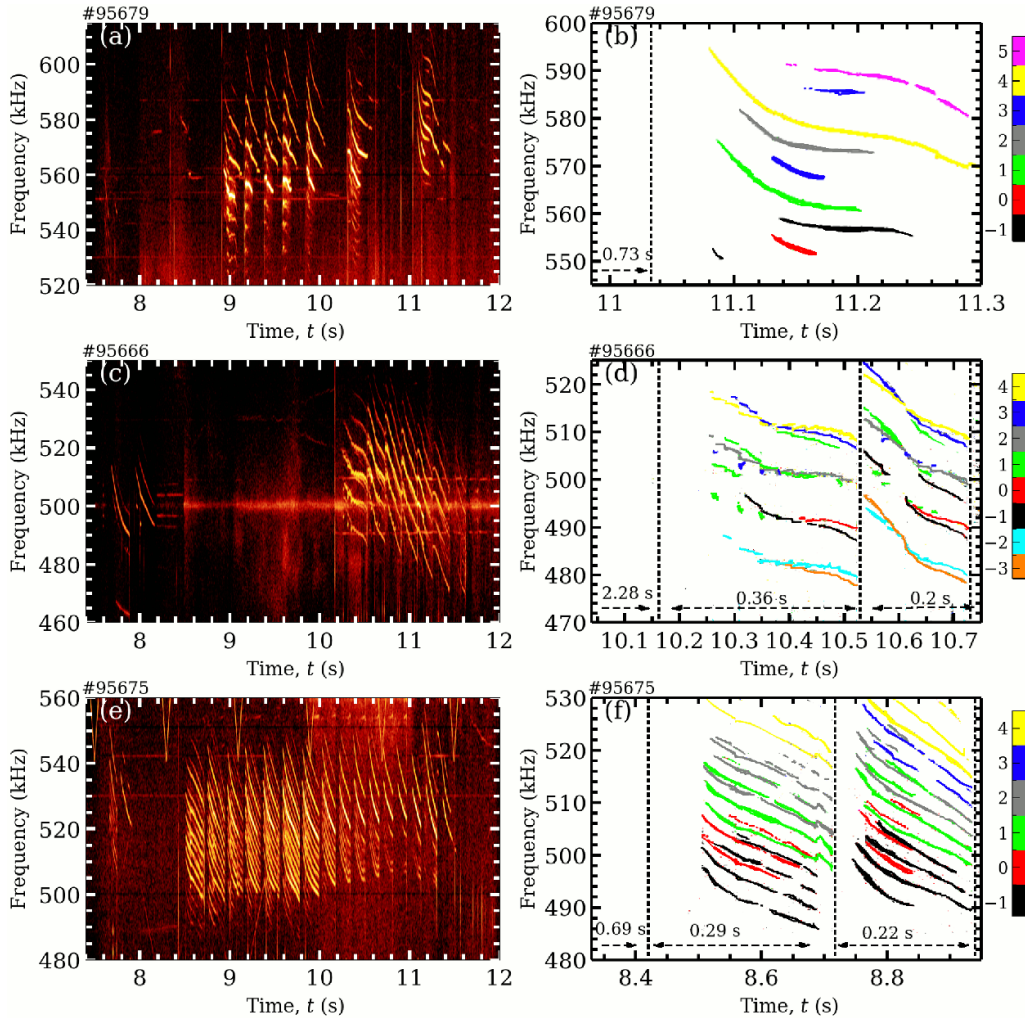
In the JT-60U experiments mentioned above, only EAEs with positive toroidal mode numbers  $n = 3-6$  were observed [35]. However, in the JET D-<sup>3</sup>He experiments described here, EAEs with lower positive  $n$ , as well as  $n = 0$  modes and even EAEs with negative toroidal mode numbers were detected. In what follows, we focus our analysis on the  $n = -1$  EAEs and axisymmetric  $n = 0$  AEs [36] as shown in the magnetic spectrograms of figure 12. The  $n = 0$  AE can only be excited if a fast-ion population is present in the plasma with an energy distribution where  $\partial f/\partial E > 0$  (so-called ‘bump-on-tail distribution’) at rather high energies for  $v_{\parallel} = v_A$  [17]. The simultaneous observation of these modes requires a large number of highly energetic counter-passing ions with such a ‘bump-on-tail’ distribution [37].

Note that fundamental ICRF minority heating leads to a Maxwellian energy distribution function  $f(E) \propto \exp(-E/T)$  with an energetic tail characterised by  $\partial f/\partial E < 0$ . The three-ion D-NBI RF heating scenario used in the experiments discussed here creates a population of accelerated D-ions with  $v_{\parallel}/v > 0$  in the range  $E_D > 0.8$  MeV, which is different from a Maxwellian distribution, but it is also characterised by  $\partial f_D/\partial E < 0$ .

The birth energy distribution of fusion products, i.e. D-<sup>3</sup>He alpha-particles, can be approximated by a Gaussian distribution function [38] with a low energy wing characterised by  $\partial f_\alpha/\partial E > 0$ . The alpha-particle birth distribution function,  $f_\alpha(E, \lambda)$  also depends on the pitch  $\lambda = v_{\parallel}/v$  as already discussed above and illustrated in figure 10. The relaxation of the birth alpha-particle distribution to the steady-state distribution, which does not have a ‘bump’ in energy space, i.e.  $\partial f_\alpha/\partial E < 0$ , occurs on the time scale of the characteristic slowing-down time,  $\tau_\alpha^* = (\tau_{se}/3) \ln(1 + (E_0/E_c)^{3/2})$ , where  $\tau_{se}$  is the Spitzer slowing-down time,  $E_0 \approx 3.6$  MeV and

**Table 1.** Main plasma parameters of discharges from figure 12.

JET pulse number	$P_{\text{NBI}}$ (MW)	$P_{\text{ICRH}}$ (MW)	$T_e(0)$ (keV)	$n_e(0)$ ( $10^{19} \text{ m}^{-3}$ )	$X[{}^3\text{He}]$ (%)
95666	8.0	5.6	7	7	25
95675	6.3	3.3	7.5	6	21
95679	6.9	5.8	7.6	5	22


**Figure 12.** Magnetic spectrograms together with toroidal mode numbers for AEs detected in discharges #95675, #95666 and #95679 (see table 1 with plasma parameters).

$E_c \approx 41T_e$  is the initial and the critical energy for the alpha-particles. Thus, the ratio  $\Delta t_{\text{ST}}/\tau_\alpha^*$  could be used as a parameter to characterise the time evolution of the distribution function of the fusion-born alphas [39]. In our experiments in D- ${}^3\text{He}$  plasmas, it varies between  $\Delta t_{\text{ST}}/\tau_\alpha^* < 1$  and  $\Delta t_{\text{ST}}/\tau_\alpha^* \gg 1$  at  $\tau_\alpha^* \approx 400$  ms.

One of the most significant observations in our experiments is a periodic modulation of the D- ${}^3\text{He}$  fusion source during short-period sawtooth phases (see figure 6), when the redistribution and the losses of the fast D-ions prevent the formation of a steady-state slowing down distribution for the fusion-born alpha-particles. One can compare this to a series of alpha-particle birth blips that lead to an energy distribution with  $\partial f_\alpha/\partial E > 0$ , i.e. the ‘bump-on-tail’ energy distribution. Also,

the observation of strong alpha-particle losses is crucial for the understanding of the destabilisation of the axisymmetric  $n = 0$  AEs. Indeed, figure 13 shows the waveform of the FILD photomultiplier, which represents first orbit losses of alpha-particles with energy  $E_\alpha > 4.5$  MeV. The spike in the alpha-particle losses followed by the post-sawtooth decrease in the losses indicates a relaxation of the alpha-particle energy distribution similar to that before the sawtooth crash. This sawtooth crash strongly disturbs the alpha-particle distribution function, making a sort of notch in the established monotonic distribution function and building up the non-monotonic phase with  $\partial f_\alpha/\partial E > 0$ . A detailed analysis of the condition  $\partial f_\alpha/\partial E > 0$  for  $v_{\parallel,\alpha} = v_A$ , which is required to excite the axisymmetric  $n = 0$  modes, is discussed in section 5.



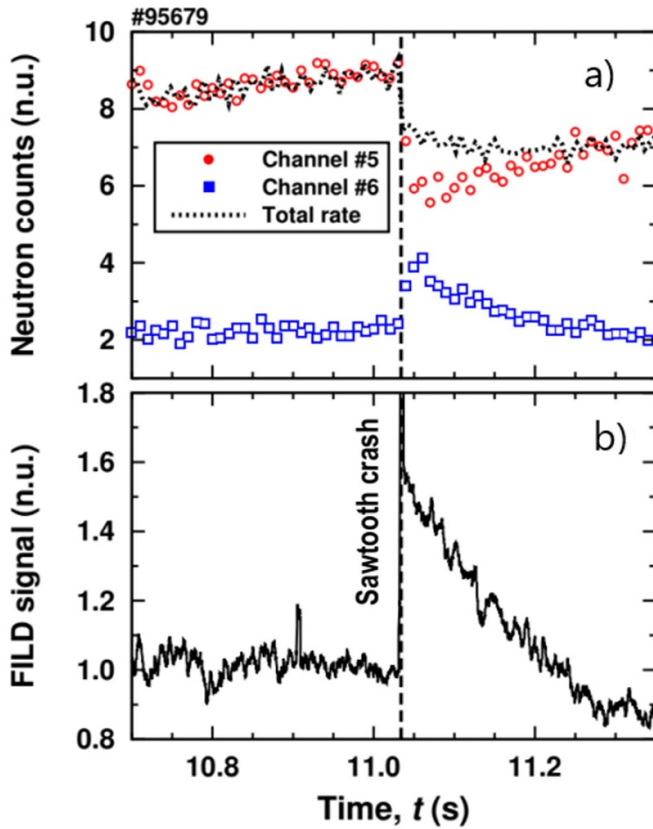


**Figure 13.** (a) Time evolution of the total neutron rate and rates in the central (#5) and outer (#6) channels of the neutron camera; (b) FILD alpha-particle losses with  $E_\alpha > 4.5$  MeV before and after the monster sawtooth crash at  $t = 11.03$  s.

#### 4. Linear stability analysis

AEs are destabilized by energetic ions through the energy transfer between resonant particles and AEs [16]. The necessary condition for a resonant wave-particle interaction is given by  $\omega = n\omega_\varphi - p\omega_\theta$ , where  $\omega$  and  $n$  are the AE frequency and the toroidal mode number;  $\omega_\varphi$  and  $\omega_\theta$  are the toroidal and poloidal orbital frequencies;  $p$  is an integer. The destabilization of AEs is only possible when the mode drive by the fast-ions is sufficiently large and overcomes mode damping by other mechanisms.

Figure 14(a) shows the computed efficiency of the resonant wave-particle interaction for the observed  $n = -1$  EAE at  $f \approx 555$  kHz in discharge #95679 (see figure 12(b)). The efficiency is obtained by calculating the variance of test-particle energy due to work done by the eigenmode electric field over many wave periods. The computations have been carried out using the HAGIS [40] and MISHKA [41] codes for a typical fixed mode amplitude  $\delta B/B = 1 \times 10^{-5}$  supposing that the  $n = -1$  EAE is interacting with energetic D-ions.

From the plotted efficiency for the wave-particle interaction in figure 14(a), the drive of the mode with a negative toroidal mode number would require the presence of a large population of energetic counter-moving D-ions ( $v_{\parallel} < 0$ ) in the plasma. The energy range for fast D-ions has been limited to

$\approx 2.5$  MeV, reflecting the experimental observations from the fast-ion diagnostics.

The two most prominent power transfer lines in figure 14(a) have been labelled to show the corresponding wave-particle resonances identified for different  $p$ -numbers in the equation, confirmed by computing the toroidal and bounce frequencies of the test-particles. The computations show that the observed  $n = -1$  EAE receives energy most effectively from fast counter-passing ions via the  $p = 0$  ( $\omega = -\omega_\varphi$ ) and the  $p = +1$  ( $\omega = -\omega_\varphi - \omega_\theta$ ) resonances. As the toroidal and poloidal orbital frequencies for passing fast-ions are given by  $\omega_\varphi = v_{\parallel}/R$  and  $\omega_\theta = v_{\parallel}/qR$  [16],  $n = -1$  modes interact effectively with these fast-ions at parallel velocities  $v_{\parallel} = -\omega R$  and  $v_{\parallel} = -\omega R/(1 + 1/q) \approx -\omega R/2$ .

For  $f_{\text{EAE}} = 555$  kHz as in discharge #95679 (figure 12(b)), one gets  $v_{\parallel} \approx -1.1 \times 10^7$  m s $^{-1}$  and  $v_{\parallel} \approx -5.4 \times 10^6$  m s $^{-1}$ , respectively. For fast D-ions, these velocities correspond to energies of  $\approx 1.2$  MeV and  $\approx 0.3$  MeV. We should note that weak higher-order wave-particle resonances for  $p = +2, +3, \dots$  are also visible in figure 14(a), but only at negative pitches and at high D-ion energies. An important remark is that while the  $p = +2$  resonance can be formally identified for particles with a positive pitch, the energy transfer between these D-ions with  $v_{\parallel} > 0$  and the  $n = -1$  mode is several orders of magnitude less efficient and thus not visible in figure 14(a).

It is important to note that the three-ion D-(D<sub>NBI</sub>)- $^3\text{He}$  ICRF scenario, which is used to accelerate fast D-NBI ions in the vicinity of the IHH layer in the mixed D- $^3\text{He}$  plasmas, is strongly selective on the sign of the parallel velocity for the resonant D-NBI ions. This is supported by TRANSP modelling confirming the preferential acceleration of fast D-ions with  $v_{\parallel}/v > 0$  and clearly showing the absence of counter-passing energetic D-ions with  $E_D$  (MeV)  $\gtrsim 0.8$  and  $v_{\parallel}/v < 0$  required to excite  $n = -1$  EAEs under these conditions. In contrast, the birth velocity distribution of D- $^3\text{He}$  fusion-born alpha-particles shown in figure 10, has a rather large broadening in energy space  $2 \lesssim E_\alpha$  (MeV)  $\lesssim 7$  with a pitch parameter  $v_{\parallel}/v$  covering the full range from  $-1$  to  $+1$ . Thus, fusion-born counter-passing alphas with  $v_{\parallel}/v \approx -1$ , rather than ICRF-accelerated fast D-ions, are a natural choice for the fast-ion species that drive the observed EAEs with  $n = -1$ .

As follows from the analysis presented above, the energy transfer between the counter-passing fast-ions with  $v_{\parallel} \approx -1.1 \times 10^7$  m s $^{-1}$  and  $v_{\parallel} \approx -5.4 \times 10^6$  m s $^{-1}$  and  $n = -1$  EAEs is the most efficient. The map showing the efficiency of the resonant wave-particle interaction for alpha-particles as a function of their energy and pitch, is shown in figure 14(b). Note that it is similar to the one for fast D-ions (figure 14(a)), but the corresponding wave-particle resonances are shifted towards higher fast-ion energies as a result of the higher mass of the alpha-particles. As follows from the figure, counter-passing alphas with energies  $E_\alpha \approx 2$  MeV provide the strongest drive for the  $n = -1$  EAE mode. These particles are naturally present in the plasma, originating from the D- $^3\text{He}$  fusion reactions. As a side remark, note that in these fast-ion experiments we obtained alpha-particle production rates comparable to or even higher than the D-D neutron rates. For example, a neutron rate of  $\sim 1 \times 10^{16}$  s $^{-1}$  was achieved



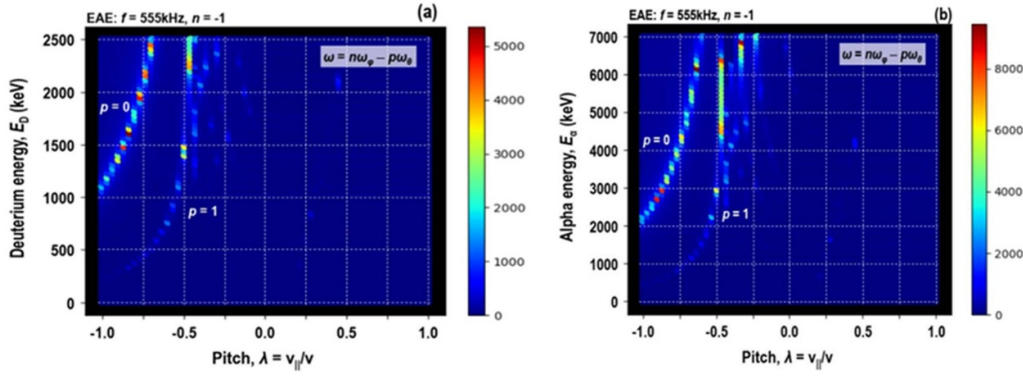


**Figure 14.** Resonance maps for observed  $n = -1$  EAE ( $f_{\text{EAE}} \approx 555$  kHz as in discharge #95679) showing the resonances for  $p = 0, +1$  for (a) D-ions and (b) alpha-particles. The computations have been carried out using the HAGIS and MISHKA codes for a fixed mode amplitude  $\delta B/B = 10^{-5}$ . Weak higher-order wave-particle resonances for  $p = +2, +3 \dots$  are also visible, but only at negative pitches and high ion energies.

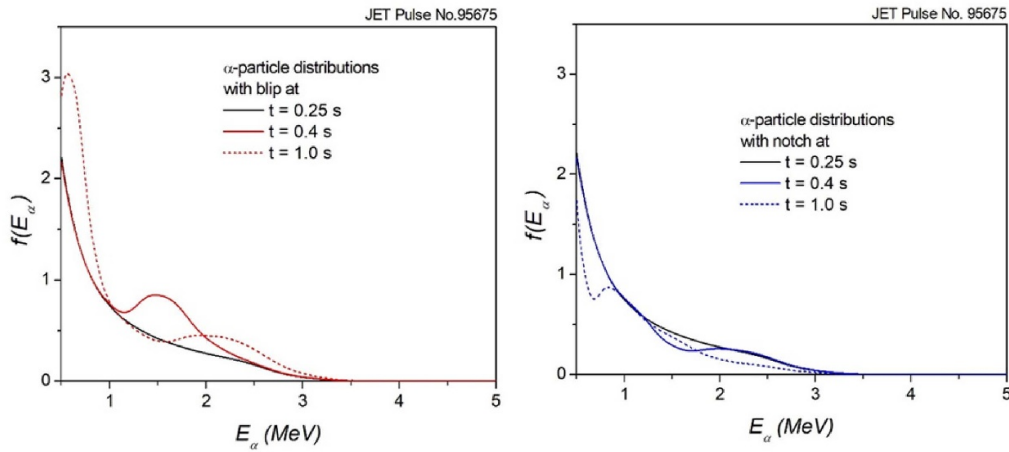


**Figure 15.** Temporal evolution of the  $f_{\alpha}(E)$  function for a blip and a notch set at the moment of the sawtooth crash ( $t = 0$  s) in discharge #95675; slowing-down of alpha-particles were calculated with the birth spectrum for  $v_{\parallel}/v = -1$  (see figure 10).

in JET pulse #95679, while the D-<sup>3</sup>He fusion rate (and thus alpha production rate) was estimated to be  $\sim 1.5 \times 10^{16} \text{ s}^{-1}$  (see figure 1(b)).

## 5. Fokker–Planck calculations

Both the sawtooth redistribution of fast D-ions and the massive prompt losses of the fusion-born alpha-particles after a sawtooth crash, lead to a periodic modulation of the fusion alpha-particle source, in turn leading to a ‘bump-on-tail’ energy distribution function with  $\partial f_{\alpha}/\partial E > 0$ .

Considering the slowing-down of fusion-born alphas in the MeV-energy range ( $2 \lesssim E_{\alpha} \text{ (MeV)} \lesssim 7$ ), the electron friction is the dominant term in the Fokker–Planck equation, describing the relaxation of the alpha-particle energy distribution. Since the alpha-particle energies are significantly larger than the critical energy ( $E_c \approx 0.3$  MeV), the fast-ion drag, the pitch-angle scattering and energy diffusion are negligible. At these high energies, the fusion-born alphas with different pitch values are gradually decelerated in collisions with electrons

without changing their  $v_{\parallel}/v$ , and this relaxation can be described by the equation  $\partial f_{\alpha}/\partial t = \tau_{\alpha}^{-1} v^{-2} \partial [v^3 f_{\alpha}]/\partial v + S_{\alpha}(v, t)$ , where  $\tau_{\alpha}$  is the Spitzer slowing-down time;  $S_{\alpha}$  is the source term for alphas. Using the alpha-particle birth spectrum shown in figure 10 as an initial condition for the above equation, the deceleration process of alphas due to the electron drag can be easily solved numerically.

Using this simplified model, we calculated the temporal evolution of the alpha-particle distribution function,  $f_{\alpha}(E)$ , just after sawtooth crashes in discharges #95675 and #95679 (see figure 12). To create a modulation of the alpha-particle source due to the sawtooth crashes, both blips and notches with a duration of 50 ms were triggered exactly at the time of the sawtooth crash, as soon as the steady-state distribution function with  $\partial f_{\alpha}/\partial E < 0$  was established. The counter-passing alpha-particle source spectrum with  $v_{\parallel}/v = -1$  was used (see figure 10). For clarity, we assumed that both the blip amplitude and depth of the notch wells are equal to  $1/2$  of the source rate. Figure 15 shows  $f_{\alpha}(E)$  distributions for the case of discharge #95675 computed at  $t = 0.25, 0.4$  and  $1$  s after the blip/notch. One can see that in both cases the perturbed alpha-particle

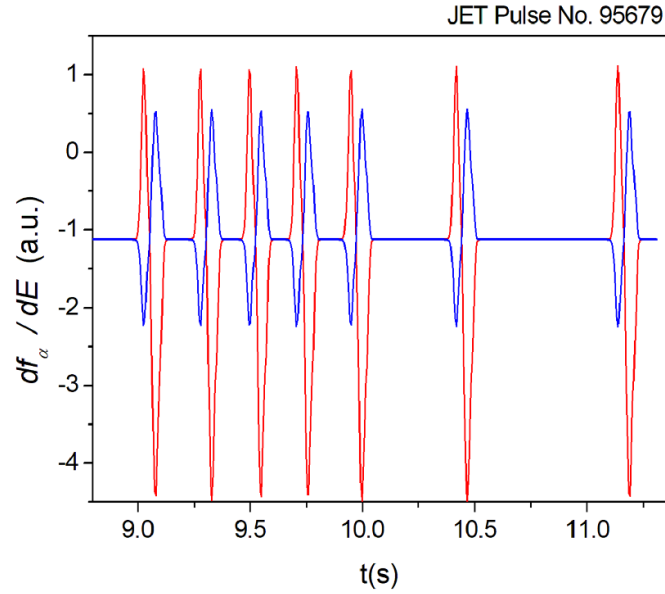


**Figure 16.** Computed temporal evolution of the  $\partial f_\alpha/\partial E$  function for blips (red line) and notches (blue line) set at sawtooth crashes in discharge #97679.

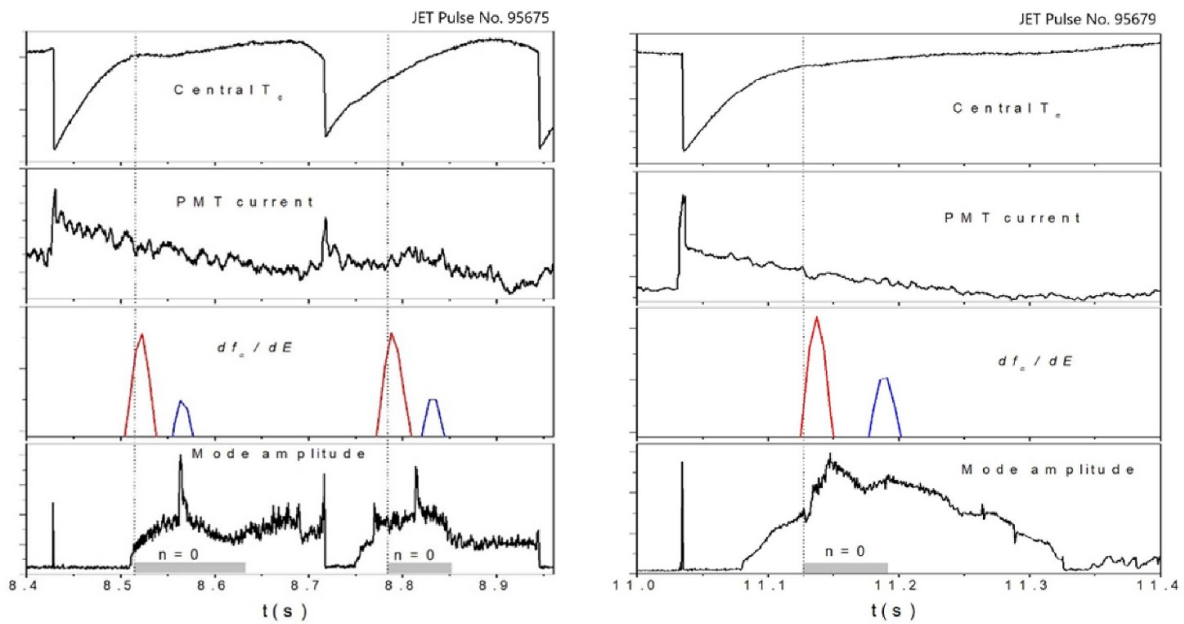


**Figure 17.** Comparison of the time evolution of  $T_{e0}$ , FILD PMT#11 currents,  $\partial f_\alpha/\partial E$  (red—blips, blue—notches) and mode amplitudes (grey bars—periods where the  $n=0$  mode is present) during sawteeth in discharges #95765 and #95679 (see figure 12); dotted lines mark the onset of the  $n=0$  AEs.

distribution functions develop a characteristic ‘bump-on-tail’ shape with  $\partial f_\alpha/\partial E > 0$ .

It is interesting to note that a notch produces a ‘bump-on-tail’ shape in the slowing-down distribution function with a delay compared to a blip. This is shown in figure 16, where the temporal evolution of the derivative  $\partial f_\alpha/\partial E$  is given for ‘bump-on-tail’ distribution functions resulting from blips and notches distribution functions. Note that the maxima for the positive derivatives are linked to counter-passing alpha-particles decelerated to resonance energies  $E_\alpha = E_A \approx 1.3$  MeV for  $v_{\parallel,\alpha} = v_A$ . This modelling can

explain the systematic periodic observations of axisymmetric  $n=0$  AEs in the experiments in D-<sup>3</sup>He plasmas discussed here.

To understand the dynamics of the  $n=0$  AEs, figure 17 shows the temporal dependency of the calculated blip/notch derivatives ( $\partial f_\alpha/\partial E > 0$ ) together with the waveforms of the central temperature  $T_{e0}$ , the FILD-PMT currents (the same as in figure 13(b)) and the AE amplitudes during sawteeth for the discharges #95675 and #95679. The mode amplitudes were obtained calculating a root-mean-square deviation in the time-dependent window ( $\approx 3$  ms) for smoothing the mode

amplitude noise. To separate the modes from other fluctuations, a band-pass 500–540 kHz filter (2nd order Butterworth filter) was used for discharge #95675 and 565–600 kHz for discharge #95679.

From figure 17 it follows that the positive part of the blip derivatives  $\partial f_\alpha / \partial E$  coincides with the onset of the  $n = 0$  modes mimicking the delay between the sawtooth crash and the AE excitation observed in the experiments. In addition, the positive part of the notch derivatives coincides with the  $n = 0$  modes providing additional energy to stabilise the mode. In fact, this is a synergetic effect between the substantial redistribution of the fast D-ions and prompt losses of fusion-born alpha-particles due to sawtooth crashes with short periods  $\Delta t_{ST} / \tau_\alpha^* < 1$ . These results, obtained with a simplified model of the alpha-particle source modulation, are fully consistent with our observations. We conclude that the conditions in our experiments create indeed a self-sustained ‘bump-on-tail’ fusion-born alpha-particle energy distribution.

## 6. Summary and conclusions

In this paper we show that fusion-born alpha-particles from the D-<sup>3</sup>He reaction are able to excite AEs with toroidal mode numbers  $n = -1$  and  $n = 0$ . The D-<sup>3</sup>He reaction, with a birth energy and kinematics for alpha-particles very similar to those released in D-T reactions but with relatively low neutron production, allows the use of fast-ion diagnostics that are incompatible with the high neutron flux environment of D-T experiments.

In our experiments we demonstrate that only the fusion-born  $\alpha$ -particles can effectively excite  $n = -1$  EAEs, confirmed by a linear stability analysis.

We propose a theoretical mechanism and provide experimental evidence for the formation of a bump-on-tail distribution for the fusion alphas required to excite  $n = 0$  AEs, which is self-sustained by a periodic modulation of the fusion source due to sawtooth crashes. The mechanism for a persisting bump-on-tail distribution of the resonant fast-ions exciting AEs is very similar to the one applied in recent NBI experiments in DIII-D, where short beam modulation periods were applied to create transiently a ‘bump-on-tail’ velocity distribution for the beam ions [42]. However, in the JET experiments in D-<sup>3</sup>He plasmas reported here, such a mechanism is self-sustained since the source rate of fusion-born alpha-particles was modulated by the sawtooth crashes.

The Alfvén instability is a significant issue for high-Q operation in ITER. Indeed, the excitation and interaction of fusion-born alpha-particles with  $n = -1$  and  $n = 0$  modes in the EAE frequency range studied in these experiments is important for the development of magnetic fusion reactors since the consequences on fast-ion transport and confinement can be substantial.

Based on the experimental and theoretical analysis of fast-ion experiments in D-<sup>3</sup>He plasmas presented here, we are planning a special scenario for demonstrating alpha-driven AEs in the forthcoming JET D-T plasma studies. The principal idea is to realize the conditions at which the energy

distribution function of fusion-born alphas is far from the steady-state distribution and has a ‘bump-on-tail’ in the Alfvénic energy range. As demonstrated in this paper, this can be achieved by modulating the alpha-particle source rate on a time scale shorter than their characteristic slowing-down time,  $\Delta t_{ST} / \tau_\alpha^* < 1$ . Thus, we propose an experiment, in which NBI power in D-T plasmas is modulated with a period shorter than  $\tau_\alpha^*$ , a similar experiment as the one in deuterium plasmas on DIII-D [42]. Demonstrating alpha-particle driven AEs with a periodic modulation of NBI power in D-T plasmas with NBI-only heating is the most straightforward way as it rules out any other possibilities for fast-ion drive.


## Data availability statement

The data that support the findings of this study are available upon reasonable request from the authors.

## Acknowledgments

This work has been carried out within the framework of the EUROfusion Consortium and has received funding from the Euratom research and training programme 2014–2018 and 2019–2020 under Grant Agreement No. 633053 and from the RCUK Energy Programme (Grant No. EP/T012250/1). To obtain further information on the data and models underlying this paper please contact PublicationsManager@ukaea.uk. The views and opinions expressed herein do not necessarily reflect those of the European Commission.

## ORCID iDs

V G Kiptily  <https://orcid.org/0000-0002-6191-7280>  
 Ye O Kazakov  <https://orcid.org/0000-0001-6316-5441>  
 M Nocente  <https://orcid.org/0000-0003-0170-5275>  
 J Ongena  <https://orcid.org/0000-0001-7456-4739>  
 M Dreval  <https://orcid.org/0000-0003-0482-0981>  
 J Eriksson  <https://orcid.org/0000-0002-0892-3358>  
 D Rigamonti  <https://orcid.org/0000-0003-0183-0965>  
 A Sahlberg  <https://orcid.org/0000-0002-9898-062X>  
 J Garcia  <https://orcid.org/0000-0003-0900-5564>  
 S E Sharapov  <https://orcid.org/0000-0001-7006-4876>

## References

- [1] Sharapov S E *et al* 2013 *Nucl. Fusion* **53** 104022
- [2] Hawryluk R J *et al* 1994 *Phys. Rev. Lett.* **72** 3530
- [3] JET Team (prepared by P.R. Thomas) 1999 *Nucl. Fusion* **39** 1619
- [4] Joffrin E *et al* 2019 *Nucl. Fusion* **59** 112021
- [5] Garcia J *et al* 2019 *Nucl. Fusion* **59** 086047
- [6] Dumont R J *et al* 2018 *Nucl. Fusion* **58** 082005
- [7] Bosch H-S and Hale G M 1992 *Nucl. Fusion* **32** 611–31
- [8] Kazakov Y O *et al* 2017 *Nat. Phys.* **13** 973–8
- [9] Ongena J *et al* 2017 *EPJ Web Conf.* **157** 02006
- [10] Kazakov Y O *et al* 2020 *Nucl. Fusion* **60** 112013
- [11] Nocente M *et al* 2020 *Nucl. Fusion* **60** 124006
- [12] Brambilla M 1999 *Plasma Phys. Control. Fusion* **41** 1

- [13] Budny R V 1994 *Nucl. Fusion* **34** 1247
- [14] White R B, Rutherford P H, Colestock P and Bussac M N 1988 *Phys. Rev. Lett.* **60** 2038
- [15] Porcelli F, Boucher D and Rosenbluth M N 1996 *Plasma Phys. Control. Fusion* **38** 2163–218
- [16] Heidbrink W W 2008 *Phys. Plasmas* **15** 055501
- [17] Kiptily V G *et al* 2021 *Nucl. Fusion* **61** 114006
- [18] Kiptily V G, Cecil F E and Medley S S 2006 *Plasma Phys. Control. Fusion* **48** R59–R8
- [19] Nocente M *et al* 2020 *Plasma Phys. Control. Fusion* **62** 014015
- [20] Rigamonti D *et al* 2018 *Rev. Sci. Instrum.* **89** 10I116
- [21] Kiptily V G *et al* 2010 *Nucl. Fusion* **50** 084001
- [22] Tardocchi M *et al* 2011 *Phys. Rev. Lett.* **107** 205002
- [23] Salewski M *et al* 2017 *Nucl. Fusion* **57** 056001
- [24] Kiptily V G *et al* 2018 *Nucl. Fusion* **58** 014003
- [25] Gatu Johnson M *et al* 2008 *Nucl. Instrum. Methods Phys. Res. A* **591** 417–30
- [26] Loughlin M J *et al* 1999 *Rev. Sci. Instrum.* **70** 1123
- [27] Ongena J P H E, Voitsekhovitch I, Evrard M and McCune D 2012 *Fusion Sci. Technol.* **61** 180–9
- [28] Pankin A, McCune D, Andre R, Bateman G and Kritiz A 2004 *Comput. Phys. Commun.* **159** 157–84
- [29] Grierson B A *et al* 2018 *Fusion Sci. Technol.* **74** 101–15
- [30] Jacobsen A S, Salewski M, Eriksson J, Ericsson G, Korsholm S B, Leipold F, Nielsen S K, Rasmussen J and Stejner M 2015 *Nucl. Fusion* **55** 053013
- [31] Jacobsen A S, Binda F, Cazzaniga C, Eriksson J, Hjalmarsson A, Nocente M, Salewski M and Tardini G 2017 *Rev. Sci. Instrum.* **88** 073506
- [32] Nocente M 2012 Neutron and gamma-ray emission spectroscopy as fast-ion diagnostics in fusion plasmas *PhD Thesis* Università degli Studi di Milano-Bicocca
- [33] Evaluated nuclear data (available at: [www.oecd-nea.org](http://www.oecd-nea.org))
- [34] Nocente M, Gorini G, Källne J and Tardocchi M 2010 *Nucl. Fusion* **50** 055001
- [35] Kramer G J, Cheng C Z, Kusama Y, Nazikian R, Takeji S and Tobita K 2001 *Nucl. Fusion* **41** 1135
- [36] Oliver H J C, Sharapov S E, Breizman B N and Zheng L-J 2017 *Phys. Plasmas* **24** 122505
- [37] Berk H L, Breizman B N and Ye H 1992 *Phys. Rev. Lett.* **68** 3563
- [38] Brysk H 1973 *Plasma Phys.* **15** 611
- [39] Kiptily V G, Baranov Y F, Barnsley R, Bertalot L, Hawkes N C, Murari A, Popovichev S, Sharapov S E, Stork D and Yavorskij V 2004 *Phys. Rev. Lett.* **93** 115001
- [40] Pinches S D *et al* 1998 *Comput. Phys. Commun.* **111** 133–49
- [41] Mikhailovskii A B *et al* 1997 *Plasma Phys. Rep.* **23** 844–57
- [42] Van Zeeland M A *et al* 2021 *Nucl. Fusion* **61** 066028